ACS APPLIED MATERIALS & INTERFACES

Research Article

www.acsami.org

Advances in Use of Capsule-Based Fluorescent Sensors for Measuring Acidification of Endocytic Compartments in Cells with Altered Expression of V-ATPase Subunit V_1G_1

Maria De Luca,[†,§] Marzia M. Ferraro,[†,‡,⬡] Raimo Hartmann,[†,⊥] Pilar Rivera-Gil,[⊥,○] Andreas Klingl,[#,△] Moritz Nazarenus,[⊥] Agnese Ramirez,[⊥] Wolfgang J. Parak,[⊥,∥] Cecilia Bucci,*[,§] Rosaria Rinaldi,[‡,□] and Loretta L. del Mercato*[,‡,⬡]

[§]Dipartimento di Scienze e Tecnologie Biologiche ed Ambientali (DiSTeBA), Università del Salento, Via Monteroni, 73100, Lecce, Italy

[‡]Istituto Nanoscienze − CNR and [□]Dipartimento di Matematica e Fisica "Ennio De Giorgi", via per Arnesano, 73100, Lecce, Italy

[⊥]Fachbereich Physik, Philipps-Universität Marburg, Renthof 7, 35037, Marburg, Germany

[#]LOEWE Centre for synthetic Microbiology (Synmikro) and Department of Cell Biology, Philipps-Universität Marburg, Karl-von-Frisch-Strasse 8, 35043, Marburg, Germany

[∥]CIC biomaGUNE, Parque Tecnológico de San Sebastián, Ed. P° Miramón 182, 20009, San Sebastian, Spain

Supporting Information

ABSTRACT: Acidification of eukaryotic cell compartments is accomplished by vacuolar H^+-ATPases (V-ATPases), large multisubunit complexes able to pump protons into the lumen of organelles or in the extracellular medium. V-ATPases are involved in a number of physiological cellular processes, and thus regulation of V-ATPase activity is of crucial importance for the cell. Indeed, dysfunction of V-ATPase or alterations of acidification have been recently recognized as key factors in a variety of human diseases. In this study, we applied capsule-based pH sensors and a real-time tracking method for investigating the role of the V_1G_1 subunit of V-ATPases in regulating the activity of the proton pump. We first constructed stable cell lines overexpressing or silencing the subunit V_1G_1. Second, we used fluorescent capsule-based pH sensors to monitor acidification before and during internalization by modified and control living cells. By using a simple real-time method for tracking capsule internalization, we were able to identify different capsule acidification levels with respect to each analyzed cell and to establish the kinetics for each. The intracellular pH measurements indicate a delay in acidification in either V_1G_1-overexpressing or V_1G_1-silenced cells compared to controls. Finally, in an independent set of experiments, we applied transmission electron microscopy and confocal fluorescence microscopy to further investigate the internalization of the capsules. Both analyses confirm that capsules are engulfed in acidic vesicular structures in modified and control cell lines. The use of capsule-based pH sensors allowed demonstration of the importance of the V_1G_1 subunit in V-ATPase activity concerning intravesicular acidification. We believe that the combined use of these pH-sensor system and such a real-time method for tracking their internalization path would contribute to systematically measure the proton concentration changes inside the endocytic compartments in various cell systems. This approach would provide fundamental information regarding molecular mechanisms and factors that regulate intracellular acidification, vesicular trafficking, and cytoskeletal reorganizations.

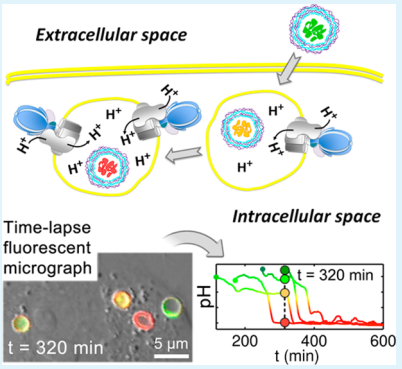

KEYWORDS: *V-ATPase, layer-by-layer microcapsules, biosensors, cell uptake, pH measurements*

INTRODUCTION

To process multiple reactions efficiently and timely, eukaryotic cells are compartmentalized into distinct membrane-bound organelles. Intracellular pH plays a pivotal role in cellular processes and is highly regulated in every organelle.[1] Indeed, proper function of a number of organelles requires acidic pH. Acidification has multiple roles: for instance, it is fundamental for ligand−receptor dissociation in endosomes, for activation of hydrolases in lysosomes, for antigen processing in immune cells, for sorting of molecules in the trans golgi network, and for neurosecretion.[2,3] Acidification of compartments is accomplished by vacuolar H^+-ATPases (V-ATPases), large multisubunit complexes that are able to pump protons into the lumen of the organelles or in the extracellular medium.[4,5] Also, the structural stability and function of proteins are tightly associated with pH.[6] For example, it has been shown that

Received: May 20, 2015
Accepted: June 18, 2015
Published: June 18, 2015

DOI: 10.1021/acsami.5b04375
ACS Appl. Mater. Interfaces 2015, 7, 15052−15060

mutations in the V-ATPase, responsible for acidification of the Golgi compartment, result in impaired glycosylation of proteins.[7] Alteration of acidification is a hallmark of a number of diseases including cancer.[8,9] In fact, in several important human diseases, such as renal tubular acidosis, osteopetrosis, diabetes, and defects in sperm maturation, acidification defects are detected.[1,5] In cancer cells, acidification is of great importance as it affects invasion properties being required for activation of secreted lysosomal hydrolases in order to degrade the extracellular matrix.[8,9] Indeed, V-ATPases are considered as promising pharmaceutical targets against development and dissemination of metastasis.[8,9] Therefore, tools to sense and monitor pH, in particular inside cellular organelles, are fundamental in order to establish how pH is regulated and, possibly, to find ways to regulate it.

Polyelectrolyte capsule-based sensors are an intriguing tool for monitoring changes of the pH inside cells and, in particular, inside endocytic organelles and lysosomes. They possess ping-pong ball-like geometry. A very thin semipermeable wall surrounds a big cavity, in which pH-sensitive fluorophores can be encapsulated.[10−12] After spontaneous uptake by cells, these capsules are mainly transported to lysosomes,[13−20] hence, they are an appropriate pH-meter for studying the regulation of pH by the proton pump V-ATPase. Recently, the suitability of such mobile, capsule-based sensors was demonstrated to detect changes in the local pH around individual capsules during the ingestion process.[12,20−25] In addition, real time monitoring of changes in the lysosomal pH of living cells has recently been demonstrated.[26]

In the present work, we investigated the importance of the V_1G_1 subunit of the V-ATPase for acidification of endocytic vesicles. This subunit is part of the peripheral stator stalk that links the peripheral cytoplasmic V_1 domain with the membrane V_0 domain of the V-ATPase,[8] and has been proposed to be important for V-ATPase assembly and functioning.[27−30] For the investigation, we constructed stable cell lines which either overexpressed V_1G_1 or were V_1G_1-silenced. Then, we tracked individual capsule-based pH sensors along their pathway from the extracellular to the intracellular environment of these cells and monitored the pH step by step. By comparing the acidification patterns among the different cell lines, the importance of the V_1G_1 subunit in V-ATPase activity could be demonstrated.

RESULTS AND DISCUSSION

Generation of Stable Cell Lines Overexpressing V_1G_1 or with V_1G_1-Silenced. To study the role of the subunit of the V-ATPase in vesicle acidification, we generated stable cell lines overexpressing HA-tagged V_1G_1 (abbreviated as HA-V_1G_1) and silencing V_1G_1 (abbreviated as sh-V_1G_1) (see Methods section). After selection with the G418 antibiotic, HA-tagged and V_1G_1-overexpressing clones were isolated. As control, we used a clone of HeLa cells stably transfected with an empty plasmid. Lysates of control and HA-V_1G_1 expressing independent clones were subjected to sodium dodecyl sulfate polyacrylamide gel electrophoresis (SDS-PAGE) and Western blot analysis using an anti-V_1G_1 antibody. The analysis revealed the presence of two bands in the HA-V_1G_1 transfected clones corresponding to the endogenous and exogenous V_1G_1, thus demonstrating V_1G_1 overexpression (Figure 1a). The HA-tagged V_1G_1 expression level was highest in clone #1. For all clones the expression of exogenous HA-tagged V_1G_1 was comparable to the endogenous level of V_1G_1. Indeed,

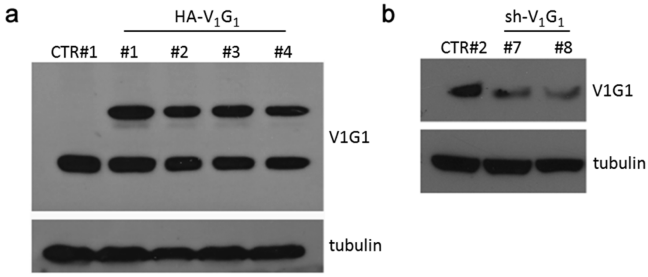

Figure 1. Expression of V_1G_1 in stable cell lines overexpressing V_1G_1 and silenced in V_1G_1. Stable cell lines were lysed and processed for Western blot analysis using an antibody against V_1G_1 to show (a) V_1G_1 overexpression or (b) V_1G_1 silencing. The numbers over the blots represent the different isolated clones. Antibodies against tubulin were used as loading control.

expression of HA-tagged V_1G_1 was similar to the endogenous V_1G_1 in clone #1, while it was about 60−80% in the other clones. In contrast, as expected, both V_1G_1-silenced cell clones showed a strong decrease of about 80% of V_1G_1 protein levels compared to control cells transfected with sh-control plasmid (Figure 1b).

Assembly and in Vitro Calibration of the Capsule-Based pH Sensors. First, we fabricated capsule-based pH sensors with encapsulated fluorescent pH indicators and reference dyes for ratiometric measurements using polyelectrolyte multilayer (PEM) capsules as carrier platform.[31,32] PEM capsules, fabricated via layer-by-layer (LbL) assembly of oppositely charged polyelectrolytes,[33] have a porous multilayered wall that surrounds a cavity.[34] The pH-sensitive dye, fluorescein isothiocyanate (FITC), and the reference dye, rhodamine B isothiocyanate (RITC), were covalently linked to dextran molecules and subsequently co-loaded into the cavities of the capsules. The attachment of the fluorophores to dextran increased their molecular weight, in order to prevent dyes from leaching out of the capsules through their semipermeable walls. The polyelectrolyte multilayer wall protects the sensor elements from interferences in the cell while allowing small molecules, in particular H^+, to diffuse into the cavity for detection.[35−37] As a result, upon ingestion of the capsule-based pH sensors, the fluorescence emission of the capsules changes depending on the local concentration of H^+ around individual capsules. Recently, the upper limit of the time response of capsule-based pH sensors was found to be below 500 ms, indicating that PEM capsules are suitable for time-resolved ratiometric pH sensing in living cells.[26,35]

Second, we tested the pH sensitivity of the capsule-based sensors under different proton concentrations (i.e., pH values). For this purpose, capsules were diluted in cell media of which the pH was adjusted between pH 2.0 and pH 8.0 (see Methods section for more details). In a subsequent step the fluorescence response was monitored via both spectrofluorimetric analysis and confocal laser scanning microscopy (CLSM) (see Figures S1 and S2 in the Supporting Information). FITC was excited at 488 nm and RITC was excited at 543 nm, and the emission signals were collected between 505 and 530 nm for the green channel and >560 nm for the red channel, respectively. By increasing the pH of the medium the overall color of the capsules shifts from "red" over "yellow" to "green" as result of the strong pH dependence of FITC (indicator dye) and the insensitivity of RITC (reference dye). The response of the capsule-based sensors can be observed in Figure 2a where the

DOI: 10.1021/acsami.5b04375
ACS Appl. Mater. Interfaces 2015, 7, 15052−15060

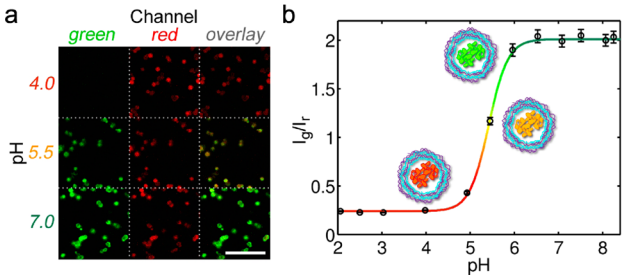

Figure 2. Calibration of capsule-based pH sensors. (a) CLSM micrographs showing the pH-dependence of capsule fluorescence in pH-adjusted cell medium (FITC was excited at 488 nm and RITC at 543 nm). Green channel (505−530 nm), red channel (>560 nm), and overlay of the fluorescence channels are reported. The size of the scale bar corresponds to 20 μm. (b) Ratiometric calibration curve of capsule-based sensors on fluorescence intensity ratio of green and red channels derived from fluorescence micrographs.

fluorescence micrographs of capsules at pH 4.0, 5.5, and 7.0 are reported. At pH 4.0 the FITC fluorescence (green channel) is very low and the overlay of the green and red channels shows red colored capsules. At pH 5.5 the FITC fluorescence increases. Accordingly, the overlay of the green and red channels shows yellow-green colored capsules. At pH 7.0, the emission of FITC increases further and in the overlay of the green and red channels capsules appear in bright green color. The intensity ratios of green and red channels were calculated for each pixel positions allocated by capsules and averaged for approximately 500 capsules/pH value. The fluorescence intensity ratio of the green and red channels derived from fluorescence micrographs were ultimately plotted as a function of pH (Figure 2b). According to literature data for ratiometric pH sensors based on FITC/RITC fluorophores,[22,23,31,38] our capsule-based pH sensors show a sigmoidal-like dependence of fluorescence, as a function of pH. The resolution of the capsule-based sensors strongly depends on the pH (see calibration curve, Figure 2b) and it is marginally limited by fluctuations of the $I_g/I_r(t)$ traces caused by photon shot noise from the imaging system. Importantly, at pH 5.5 the capsule-based sensors allow to distinguish changes of ΔpH $\approx$ 0.05, whereas for pH < 4.5 and pH > 6.5 these changes could no longer be discriminated. Nonetheless, the sensors are able to measure pH changes down to 4.5, and thus, cover the pH range of endocytic organelles and lysosomes.[39] It is worth to mention, that the dynamic pH measurement range of the capsule-based sensors can be further expanded by adding an additional pH-sensitive dye (such as Oregon Green) to the FITC and RITC dyes. By adopting this strategy, Song and colleagues demonstrated the possibility to fabricate triple-labeled microcapsules with a dynamic pH measurement range of 3.3−6.5.[22]

Intracellular pH Sensing in Cells with Modified V-ATPase. We subsequently used the above-described capsule-based pH sensors for comparing the pH along the internalization pathway in the different generated cell lines (see Figure 1). The capsule-based sensors were added to the cell culture medium of control cells, HA-V_1G_1 cells and sh-V_1G_1 cells in a ratio 15:1. Capsule uptake was followed via CLSM time-lapse microscopy up to 24 h. We used different clones (the ones indicated in Figure 1) in order to be sure that any reported effect was actually due to the expression or silencing of the V_1G_1 protein and to improve the statistics. In particular, we used clones #1, #2, #3, and #4 for HA-V_1G_1 cells, and clones #7 and #8 for sh-V_1G_1 cells. As controls, we used stably trasfected HeLa cells with pCDNA3 empty plasmid (CTR #1) and stably transfected HeLa cells with sh-control plasmids (CTR #2). Capsules are internalized by a huge variety of cells,[13−19] involving the concomitant activation of phagocytosis and lipid rafts-mediated macropinocytosis.[20] Cholesterol enriched domaines of the plasma membrane are crucial for the initial uptake and the final localization of the capsules inside phagolysosomes.[20] Furthermore, the capsules are deformed upon incorporation by cells, likely due to the mechanical pressure within the intracellular vesicles that leads to squeezing of the capsules.[19,40,41] Namely, this deformation does not impair the sensing properties of the capsules that retain both, the pH-sensitive and the reference fluorophores within their cavities. Figure 3a shows three representative time-lapse micrographs of control cells (CTR #2) at different time points (60, 180, and 220 min). The overlay of the brightfield, "green" and "red" channels show capsules with different colors because of their localization in environments with different local pH values. Precisely, the capsules in "green" color are outside the cells or attached to the cell membrane, whereas the capsules in

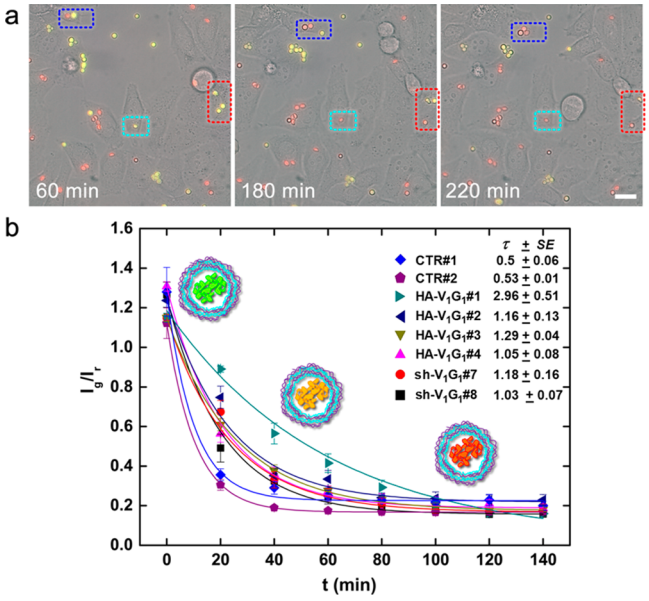

Figure 3. In vitro pH response of capsule-based sensors following cellular uptake. (a) Time-lapse fluorescence micrographs showing the color changes of capsule-based pH sensors added to control cells (CTR #2), as recorded after 60, 180, and 220 min. Before internalization, capsules display a strong green fluorescence due to the neutral pH of the cell medium. After internalization, the capsules display a strong red fluorescence due to their confinement in acidic endosomal/lysosomal compartments inside cells. Dashed rectangles highlight the color shift from green to red of capsules being internalized by cells over several hours of incubation. Images were taken in green and red fluorescence and transmission channels. The overlay of the three channels is presented in the Figure. Scale bar: 25 μm. (b) Fluorescence intensity ratios (I_g/I_r) of capsule-based sensors added to controls (CTR #1 and #2), sh-V_1G_1 and HA-V_1G_1 clones. The fluorescence of capsules was measured at different time points by time-lapse microscopy and then plotted versus time. The continuous lines are fits to the data using the function $I_g/I_r(t) = I_g/I_r(t = 0)\cdot \exp(-t/\tau) + I_g/I_r(t \rightarrow \infty)$, with the 3 fit parameters τ, $I_g/I_r(t = 0)$, and $I_g/I_r(t \rightarrow \infty)$. The bigger τ, the faster acidification occurs. The error bars represent the standard deviation calculated over 45 capsules analyzed at the indicated time points.

DOI: 10.1021/acsami.5b04375
ACS Appl. Mater. Interfaces 2015, 7, 15052−15060

"red" color are entering the cells or have already been confined into acidic intracellular vesicles. Thus, the color changes displayed by the internalized capsule-based pH sensors can be correlated to intracellular local pH changes. From the fluorescence intensity of the indicator (I_g) and reference (I_r) dyes, the I_g/I_r ratio displayed by capsules in each cell line was calculated and plotted against the time (Figure 3b). At each time point, several images were taken and over 45 capsules/sample were analyzed. Because the ingestion of capsules may occur at different time points within the same cell culture (the uptake is a statistical process over the time period), we fixed, for each individual capsule-based sensor, t_0 as the time-point in which the capsule is still located in the extracellular environment (overall green color) just before being engulfed by the cell and passed to the acidic compartments (overall yellow and red colors). As shown in Figure 3b, the two control cells (HeLa cells transfected with pCDNA3 empty vector and HeLa cells transfected with control sh-plasmid) showed similar $I_g/I_r(t)$ behaviors. In contrast, the cell lines in which the HA-tagged V_1G_1 was expressed (HA-V_1G_1, clones #1, #2, #3, and #4) showed a slower kinetic of acidification, as compared to the control cells. These findings are in agreement with previous data indicating that overexpression of this subunit inhibits maturation of the lysosomal enzyme cathepsin D,[30] and altogether suggest that lysosomal functionality is impaired in cells overexpressing V_1G_1. It is worth to note that, using these capsule-based pH sensors and following them by live microscopy, we were able to monitor precisely kinetics of acidification of the capsules together with their path in the cells and, notably, we could establish that the clone HA-V_1G_1 #1, which showed the strongest expression of HA-V_1G_1 (see Figure 1), displayed the strongest effect (although the trend was the same). These findings indicate that increasing amounts of V_1G_1 exert an increasing inhibitory effect thus suggesting a dose response effect. This is important for the future development of therapeutic means for diseases involving V-ATPase, as therapeutic strategies should take into account that expression of the right amount of V_1G_1 is fundamental to ensure the correct functioning of the pump. Indeed, also in cell lines in which V_1G_1 was silenced (sh-V_1G_1, clones #7 and #8), the kinetics of acidification were slower compared to control cells, in agreement with previous data on the importance of V_1G_1 abundance.[30]

Altogether, these data demonstrate that expression of the right amount of the V_1G_1 subunit is crucial, as overexpression or reduced expression of this subunit results in slower kinetics of acidification, and indicate that the V_1G_1 subunit is essential for the proper function of V-ATPase.

To gain deeper insight into the acidification mechanisms, we have focused our attention on the overexpressing clones #1 (HA-V_1G_1 #1) and #3 (HA-V_1G_1 #3) and the silenced clone #7 (sh-V_1G_1 #7). We have followed the uptake of single capsule-based sensors by tracking their movement from the extracellular medium to the intracellular compartments. As the two control cells showed analogous $I_g/I_r(t)$ behaviors, we have selected CTR #2 cells for the tracking analysis. We calculated the acidification time in control cells, in cells V_1G_1-overexpressing, and in V_1G_1-silenced cells (Figure 4) (see the Supporting Information for details about tracking measurements). This analysis confirmed that a delay in acidification is present both, in V_1G_1-overexpressing clones or V_1G_1-silenced clones. Furthermore, the overexpressing clone #1 showed again the slowest kinetic of acidification (Figure 4d, e). In addition,

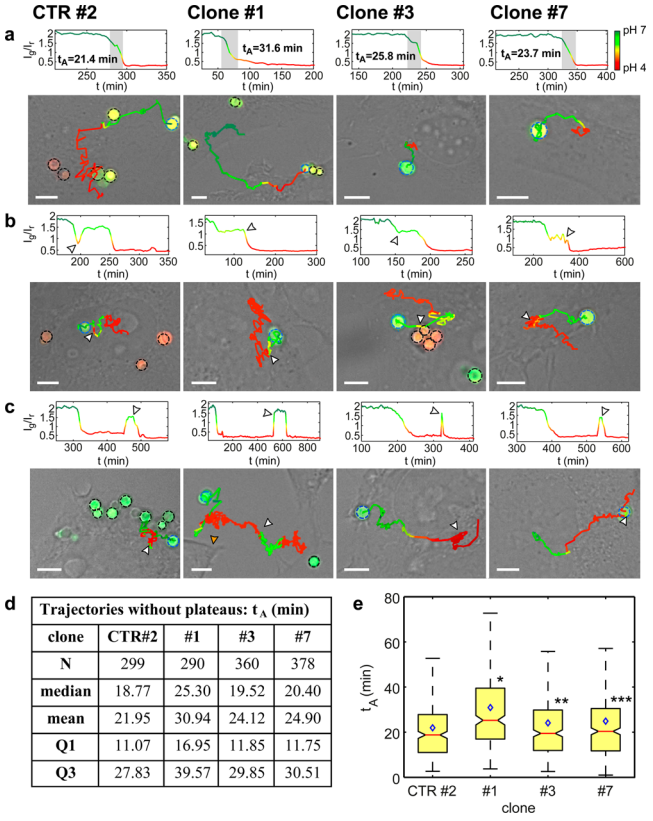

Figure 4. Real-time measurements of cell acidification by capsule-based sensors. (a) Examples of use of capsule-based sensors for real-time monitoring of acidification by tracking the fluorescence intensity of a single capsule (indicated by blue dashed regions of interest (ROIs)) from the time of initial attachment to the cell through the completion of acidification (red color). The acidification times t_A are derived from a sigmoidal fit to each individual trajectory and are representing the time period between high pH (green plateau) and low pH (red plateau) locally around each capsule. (b, c) In some cases, the acidification is not a continuous process and nodes (duration t_I), indicated by white arrows in the fluorescence images, occur at intermediate pH levels (around pH 5.6) (Figures S5–S6, Supporting Information). The size of the scale bar corresponds to 5 μm. (d) Table with number of evaluated trajectories N per clone, mean and median values for the acidification time t_A as well as the corresponding upper and lower quartiles (Q1 and Q3). (e) In the box plot, t_A is plotted for all different clones ignoring trajectories with nodes. The blue diamonds correspond to the mean values of the distribution. The acidification rate of clone #1 was significantly lower than that of the control cells ($p < 0.0001$, *). P-values were obtained from a two-tailed Wilcoxon–Mann–Whitney test. Additional significance levels: $p < 0.23$ (**), $p < 0.17$ (***).

this tracking analysis allowed us for following the capsules step by step together with their acidification state. In most cells (79%), acidification was a continuous process, as shown in Figure 4a.

The pH decrease started immediately after the engulfment of the capsules, and the FITC/RITC ratio remained fairly constant at a pH below 5.0. However, in some cells acidification was not a continuous process and showed stops at intermediate pH levels (Figure 4b and Figures S5–S6 in the Supporting Information). This trend was present in 21% of the observed capsule trajectories and could possibly be due to slower kinetics of movement toward the cell center or to slower and/or less fusion events with already more acidic vesicles. Furthermore,

DOI: 10.1021/acsami.5b04375
ACS Appl. Mater. Interfaces 2015, 7, 15052–15060

although most capsules showed a regular acidification trend while moving toward the cell center (Figure 4a), in some cases (6% of all trajectories), we could observe a sudden increase in pH followed by a rapid or slow reacidification (Figure 4c). In this case, capsules might be present in compartments that fuse with less acidic organelles, thus, increasing the local pH.

Localization of Capsule-Based pH Sensors in Cells with Modified V-ATPase. We further assessed the internalization of the capsules via transmission electron microscopy (TEM) analysis (Figure 5 and Figures S8–S11 in the Supporting Information) and CLSM analysis (Figure 6). For both methods we selected two time points, 1 and 24 h, as at this stage of our investigation we specially focused on comparing the initial and final localization of the capsules in all analyzed cells. The membranes and cristae within the mitochondria are visible and do not seem to be distorted or broken. The cytoplasm is homogeneous, showing free ribosomes, rough endoplasmic reticulum with attached ribosomes and vesicles. Within the cytoplasm, vesicular structures, most likely lysosomes and endosomes, are found. A double membrane surrounds the nucleus with regular interruptions consisting of nuclear pore complexes. Furthermore, hetero- as well as euchromatin can be distinguished. As shown in Figure 5, several capsules can be seen inside the different cell clones at 1 h and, as expected, the number of internalized capsules increased with time.

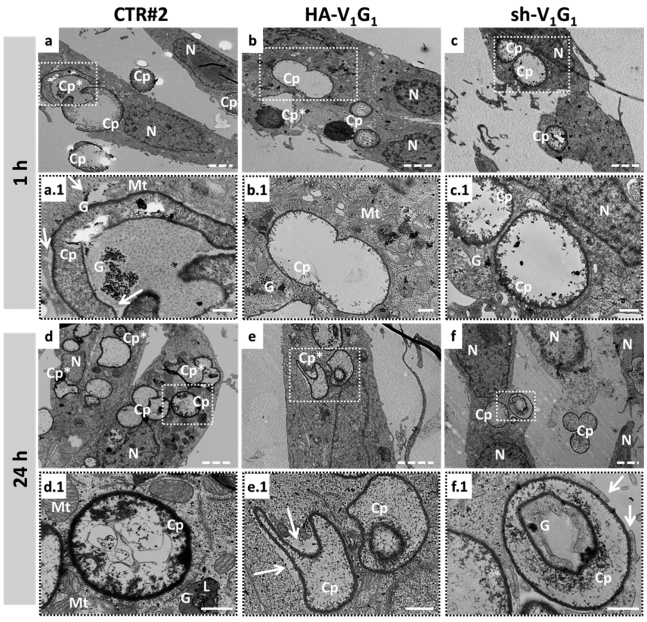

Figure 5. Internalization of PEM capsules by V_1G_1-overexpressing or V_1G_1-silenced cells. The images show the uptake of the capsules that have been added to control cells (CTR #2) and cells overexpressing (HA-V_1G_1,) or lacking (sh-V_1G_1) the V_1G_1 subunit. Images were taken after (a–c) 1 h and (d–f) 24 h of cell–capsule interaction. Cp, capsules; N, nucleus; Mt, mitochondria; G, glycogen; L, lysosome. Stars, examples of deformed capsules. Dashed box, zoomed areas of representative capsules. Solid arrow, plasma membrane surrounding the capsules. Scale bars: dashed line, 2 μm; straight line, 500 nm. For more TEM images, please see Figures S8–S11 in the Supporting Information.

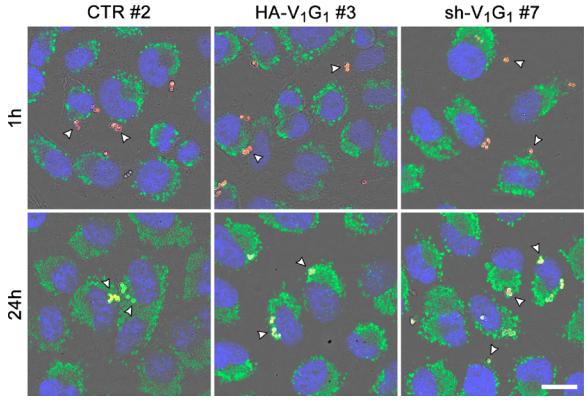

Figure 6. Co-localization of capsules internalized by V_1G_1-overexpressing or V_1G_1-silenced cells. CLSM images of control cells (CTR #2), HA-V_1G_1 cells (clone #3), and sh-V_1G_1 cells (clone #7) following 1 h (top row) and 24 h (bottom row) incubation with fluorescently labeled $(PSS/PAH)_5$ capsules (white arrows). Dex-RITC-loaded capsules (red); LAMP1 (green); DAPI staining (blue). Overlay images of red, green, blue, and transmission channels. Scale bar: 20 μm.

Internalization is a statistical process and therefore, over time, the capsules are continuously in contact with the cell membrane or within the cytoplasm, corresponding to the progress of being phagocytosed. Those capsules exhibited an electron dense outer layer due to the presence of gold nanoparticles which had been added to the capsule walls (Figures S10a.1 and S11a in the Supporting Information), and were surrounded by a lipid monolayer after internalization, indicated by the solid arrows in Figures 5a.1, e.1, and f.1 (Figures S8a.1, S8b, S9b.1, S10a.1, S10b, S11a, and S11c in the Supporting Information). The already mentioned deformation of capsules at some later point after phagocytosis was also observed in all images. The capsules were sorted to the lysosomes.[20] Examples of colocalization and merging of the lysosomes with the phagosomes can be seen in the images reported in the Supporting Information (Figures S8c, S9b.1, S10b, S10c, S11a, and S11d). From the TEM images plenty of black dots that can be identified as glycogen, could be seen in all transfected cells, especially after 1 h (Figure 5) (see also the Supporting Information). The metabolism of glycogen provides the cell with energy in form of ATP. Figure 5a.1 and f.1 shows examples of how glycogen clearly colocalizes with lysosomes containing capsules (Figures S8b-c, S10b, and S11c-d in the Supporting Information). This new situation is reversible and should not interfere with the regular cell cycle. This is in agreement with other works.[20,42] Transfected HA-V_1G_1 cells appeared more adapted to the presence of the capsules than sh-V_1G_1 cells as the reduction of the local accumulation of glycogen is slightly more advanced in these cells after 24 h. Actually, the amount of glycogen in sh-V_1G_1 cells after 24 h (Figure 5f and f.1 and Figure S11c, d in the Supporting Information) is very similar to the amount found after 1 h (Figure 5c, c.1 and Figure S11a, b in the Supporting Information).

Co-localization of the capsules with lysosomes was also confirmed by CSLM (Figure 6). Fluorescently labeled $(PSS/PAH)_5$ capsules were incubated with control cells (CTR #2), with V_1G_1-overexpressing cells, and with V_1G_1-silenced cells, for 1 and 24 h. The intracellular localization of the capsules was studied using confocal immunofluorescence analysis with antibodies against LAMP1 (lysosomal-associated membrane protein 1), a protein that resides in membranes of late endosomes and lysosomes.[43,44] At 1 h incubation time point,

DOI: 10.1021/acsami.5b04375
ACS Appl. Mater. Interfaces 2015, 7, 15052–15060

no colocalization of capsules (red) with LAMP1-positive organelles (green) was observed (Figure 6, top row). In all cells, the capsules were located in the cell periphery or close to the cell membrane, as being internalized by the cells. In contrast, at the 24 h incubation time point, the capsules were predominantly distributed around the nuclei, where lysosomes were mostly grouped. In all cells, the overall color of internalized capsules shifted from red to yellow (Figure 6, bottom row), indicative of colocalization with LAMP1-positive acidic organelles, such as late phagosomes and phagolysosomes.

CONCLUSIONS

Altogether, these data indicate the utility of capsule-based pH sensors to measure the pH inside compartments, such as phagosomes and phagolysosomes. In contrast to other methods available for measuring pH (e.g., injection of fluorescent pH indicators), the main advantage of capsule-based pH sensors lies in their final and fixed intracellular distribution. Indeed, capsules end up in the lysosomes/phagolysosomes, where they stay for long time. Therefore, they represent a valuable tool to follow acidification in living cells over time and to study the acidification process during the endocytic pathway. Furthermore, the data obtained on V_1G_1-overexpressing or V_1G_1-silenced clones demonstrate that the V_1G_1 subunit is important for V-ATPase activity confirming previous works,[27−30] and indicate that these sensors can be used to investigate V-ATPase functioning. Clearly, further work will be necessary to resolve questions about the exact role of V_1G_1 in regulation of the V-ATPase activity.

METHODS

Materials. Poly(sodium 4-styrenesulfonate) (PSS, M_w ∼70.000 Da, #243051), poly(allylamine hydrochloride) (PAH, M_w ∼56.000 Da, #283223), calcium chloride dehydrate ($CaCl_2$, M_w = 147.01 Da, #223506), sodium carbonate (Na_2CO_3, M_w = 105.99 Da, #S7795), dextran (M_w ∼ 2000.000 Da, #95771), fluorescein 5(6)-isothiocyanate (FITC, M_w = 389.38 Da, #46950), rhodamine B isothiocyanate (RITC, M_w = 536.08 Da, #R1755), and ethylenediaminetetraacetic acid disodium salt dihydrate (EDTA, #E5134) were purchased from Sigma-Aldrich. Amino dextran (AM-dextran, M_w ∼500.000 Da, #D-7144) was obtained from Invitrogen. Gold colloids 5 nm (#EM.GC15) were obtained from BBI International and bis(p-sulfonatophenyl)phenylphosphine dihydrate dipotassium salt (#15−0463) from Stream Chemicals. All chemicals were used as received. Ultrapure water with a resistance greater than 18.2 MΩ/cm was used for all experiments.

Cell Cultures. All cells were cultured in phenol-red free Dulbecco's Modified Eagles Medium (DMEM, Sigma-Aldrich, #D6546) supplemented with 10% fetal bovine serum (Biochrom, #S0615), 1% penicillin/streptomycin (Sigma-Aldrich, #P4333) and 2 mM L-glutamine (Sigma-Aldrich, #G7513) at 5% CO_2 and 37 °C.

Generation of Stable Cell Lines. Stable cell lines overexpressing and/or silencing V_1G_1 were generated using pCDNA3_2xHA-V_1G_1 or sh-RNA V_1G_1 plasmids (sc-36797-SH, Santa Cruz Biotechnology), respectively. Stable cell lines were selected by adding G-418 (1 mg/mL, Calbiochem) to cells transfected with HA-V_1G_1 or Puromycin (3 μg/mL, Sigma-Aldrich) to V_1G_1-silenced cells. Cells were kept in selective media for about 2 weeks or until clones were visible. About 10 independent clones were picked for each sample and propagated. Lysates of some of the clones were processed for Western blot analysis to verify V_1G_1 overexpression or silencing. HA control cells were transfected with an empty vector and selected with G-418, whereas sh-control cells were transfected with a control sh-plasmid and selected with puromycin. After the selection the clones overexpressing HA-V_1G_1 were cultured in medium supplemented with 0.25 mg/mL G418, whereas V_1G_1-silenced clones and control cells were maintained in medium supplemented with 0.75 μg/mL puromycin.

Western Blotting (WB). HeLa cells were lysed in RIPA buffer (Sigma-Aldrich) plus proteinase inhibitors cocktail (Roche). Lysates were loaded on SDS-PAGE and separated proteins were transferred onto PVDF membranes from Millipore. The filter was blocked in 5% milk in phosphate buffered saline (PBS) for 30 min at room temperature, incubated with the appropriate primary antibody mouse monoclonal anti-V_1G_1 (1:100, #sc-25333, Santa Cruz Biotechnology) and mouse monoclonal anti-tubulin (1:3000, clone B512, Sigma-Aldrich), and then with a secondary antibody conjugated with HRP (1:5000, #G21040 Invitrogen). Bands were visualized using Western blot Luminol Reagent (Santa Cruz).

Synthesis of Capsule-Based pH Sensors. The preparation of capsule-based pH sensors was carried out following our previous protocol.[31] Briefly, 0.615 mL of 0.33 M $CaCl_2$, 0.615 mL of 0.33 M Na_2CO_3, 0.4 mL of FITC-dextran solution (30 μM), and 0.37 mL of RITC-dextran solution (30 μM) were rapidly mixed and thoroughly agitated on a magnetic stirrer for 30 s at room temperature. After the agitation, the precipitate was separated from the supernatant by centrifugation (4500 rpm, 5 s) and washed three times with water. Then, the resulting $CaCO_3$ particles, containing FITC-dextran and RITC-dextran, were subjected to the LbL deposition of PSS (2 mg/mL, 0.5 M NaCl, pH 6.5) and PAH (2 mg/mL, 0.5 M NaCl, pH 6.5) polyelectrolytes (15 min under agitation) to give the following multilayer wall architecture: $(PSS/PAH)_5$. Short ultrasound pulses were applied to the sample prior to the addition of each polyelectrolyte in order to prevent particle aggregation. The decomposition of the $CaCO_3$ core, resulting in hollow microcapsules, was achieved by treatment with 1 mL of EDTA (0.2 M, pH 7.0) followed by triple washing with water. The microcapsules were stored as suspension in water at 4 °C.

Synthesis of Gold Nanoparticle-Functionalized Capsules. To visualize the capsules with the transmission electron microscope, we embedded electron-dense gold nanoparticles (Au-NPs) into the walls. The synthesis was carried out as follows. In a vial equal volumes (1.2 mL) of aqueous $CaCl_2$ and Na_2CO_3 solutions (0.33 M) were mixed in the presence of 1.54 mL of dextran (13 mg/mL). The solution was thoroughly mixed on a magnetic stirrer for 30 s and afterwards, the mixture was left without stirring for 3 min. After three washing steps with Milli-Q water, the resulting particles were coated with one bilayer of polyelectrolytes ($CaCO_3$@(PSS/PAH)). Then, the coated cores were functionalized with phosphine-stabilized Au-NPs following our previous protocol.[45] Afterward, 4 more bilayers of (PSS/PAH) were added. The dissolution of the cores was carried out as described above. The final architecture of the capsules was therefore (PSS/PAH)Au-NPs$(PSS/PAH)_4$. We incorporated dextran (2000 kDa) into the $CaCO_3$ cores, as dissolution of cores including dextran by addition of EDTA is faster than that of cores without dextran. Naturally, in this way, dextran remains inside capsule cavities after core dissolution.[45]

Characterizations of Capsules. Capsule size was determined from fluorescence micrographs. The diameter of the microcapsules produced was 2.6 ± 0.3 μm (N = 4130).

The Zeta potential (ζ) of the capsules was measured in Milli-Q water by dynamic light scattering (DLS) using a Zetasizer Nano ZS (Malvern Instruments, UK). The results were averaged from 3 parallel measurements. All microcapsules used in this work had a zeta potential value of 11.9 ± 0.2 mV.

The capsule number per volume was determined with a hemocytometer under an optical microscope. A drop of a diluted solution of capsules was added onto the chamber and the number of capsules in the volume defined by the hemocytometer was counted by using a 20× objective in phase contrast mode. The capsules concentration was estimated to be around 1.5×10^8 capsules mL^{-1}.

Spectrofluorometer and Confocal Intensity Titrations. For in vitro spectrofluorometric titrations, first, the pH of the cell medium was adjusted to various pH values ranging from 2.0 to 8.0 (by 1 M NaOH or 1 M HCl). The pH of the final solutions was checked with a pH meter (Professional-Meter PP-50, Sartorius). Then, 10 μL of capsules (1.5×10^8 capsules mL^{-1}) were mixed with an excess of cell

DOI: 10.1021/acsami.5b04375
ACS Appl. Mater. Interfaces 2015, 7, 15052−15060

medium to buffer ratio of about 1:10 and measured with a Fluorolog (FL3−122) fluorescence spectrometer equipped with a 450 W xenon short arc lamp (Ushio-UXL-450S−O) as the source of excitation. Emission spectra were collected at 500−550 nm ($\lambda_{excitation}$ = 488 nm) for FITC and 565−625 nm ($\lambda_{excitation}$ = 543 nm) for RITC. For in situ confocal microscopy titrations, 10 μL capsules suspension aliquots (with the same buffers used for each pH point) were pipetted on coverslips. Confocal scans were normally performed with a Leica TCS SP5 (Leica Microsystems, Germany) or, where indicated, with a CLSM 510 Meta (Zeiss, Germany). Laser power, acquisition parameters, and excitation light exposure times were adjusted to optimize signal-to-noise ratios and minimize photobleaching, and were kept constant throughout each pH titration series. FITC was excited at 488 nm with an argon laser and its fluorescence was collected between 505 and 530 nm ("green" channel). RITC was exited at 543 nm using a helium neon laser; the fluorescence was detected with a long-pass filter >560 nm ("red" channel).

Live Confocal Fluorescence Microscopy. For internalization of the capsule-based pH sensors, approximately 10 000 cells per cm^2 were seeded in a sterile microscopy chambers (8-well μ-slide, Ibidi) in complete DMEM. Before analysis, cells were incubated with 15 capsules/cell in L-15 medium (without phenol red, Leibowitz medium, GIBCO).

For capsule tracking experiments, clones #1 and #3 (overexpressing V_1G_1), clone #4 (silencing V_1G_1) and stably transfected HeLa cells with sh-control plasmids (CTR #2) were selected. 15,000 cells/well were seeded into each well of an 8-well μ-slide (Ibidi, #80826). The μ-slides were transferred to a CLSM (CLSM 510 Meta, Zeiss, Germany) equipped with a portable incubator (Pecon, Germany) and maintained at 37 °C with 5% CO_2. Immediately before image acquisition, approximately 15 capsules/cell were added and a time-lapse image series was acquired using a Plan-Apochromat 63×/1.40 Oil DIC M27 objective. To minimize the effect of photobleaching, the acquisition parameters were tuned to detect FITC/RITC-fluorescence at very low excitation power. Images were acquired with a lateral sampling frequency of 0.2 μm and a temporal resolution of 150 s. To image capsules already being internalized (a) and those still adhering to the outer plasma membrane on top of the cells (b), two images at the same lateral position but different axial positions were acquired. For (a), one slice was imaged 2.2 μm above the substrate, which was typically located in the cell interior. For (b), another image was obtained at a position 3 μm higher to resolve capsules located on top of cells. The pinhole of the confocal system was adjusted to capture 2 μm thick sections in both cases. This alignment was recovered before each time point by a software-based autofocus routine which was searching for the boundary layer μ-dish substrate/medium characterized by an increased level of scattered photons. After acquisition, the projection along the *z*-axis of both slices was calculated and used for further analysis. The described procedure resulted in almost gapless two-dimensional capsule trajectories.

Ultrastructural Analysis via Transmission Electron Microscopy (TEM). For TEM analysis, samples were chemically fixed with glutaraldehyde. For the chemical fixation protocol, the different clones were seeded in a Petri dish (Ø 100 mm) until 80% confluence and then were treated with the sensor capsules (20 capsules/cell) for 1 and 24 h. Cells were placed in the fixative solution (2.5% glutaraldehyde) for 45 min at room temperature (RT). Afterward the cells were collected with a scraper and concentrated via centrifugation, discarding the supernatant. Postfixation was performed in 1% osmium tetroxide for 1.5 h at 4 °C. Then, cells were dehydrated in grading series of acetone, infiltrated with an EPON:acetone mixture, and finally embedded in pure EPON resin. Resins were polymerized at 60 °C for 48 h. Ultrafine sections were contrasted with 2% aqueous uranyl acetate for 30 min at RT first and followed by exposure to Reynolds' lead citrate for 10 min at RT. Sections were imaged with a JEOL JEM 1010 (100 kV) transmission electron microscope equipped with a Bioscan Gatan wide angle slow scan CCD camera.

Confocal Immunofluorescence Microscopy. HeLa cells stably transfected with sh-control plasmids (CTR #2), clones HA-V_1G_1 #3, and sh-V_1G_1 #7 were selected for colocalization studies. $(PSS/PAH)_5$ capsules, carrying only dextran-RITC into the cavities, were produced by following the procedure described above. Cells were grown on 11 mm round glass coverslips; 1 and 24 h before the fixation, the cells were incubated with 15 capsules/cell in complete DMEM. Then, the cells were fixed in 3% paraformaldehyde (Sigma-Aldrich), permeabilized with piperazine-N,N′-bis(2 ethanesulfonic acid) (PIPES)-Saponin 0.1%, and incubated with primary antibodies for 1 h. After 3 washes with PBS-Saponin 0.1%, the cells were incubated for 30 min with the secondary antibodies and then with DAPI dye (1 μg/mL). The following antibodies were used: mouse anti-Lamp1 at a 1:250 dilution (#H4A3, Developmental Hybridoma Bank University of Iowa), goat anti-mouse AlexaFluor488 at a 1:500 dilution (#A11001, Invitrogen). Subsequently, cells were viewed with a CLSM microscope (TCS-SP5; Leica, Germany) equipped with a laser diode emitting at 405 nm, an argon-ion laser with a line at 488 nm, and a helium−neon laser for excitation at 543 nm. The fluorescence signal of DAPI was detected after filtering with a band-pass filter within the range 415−500 nm, the fluorescence signal of AlexaFluor488 was detected with a band-pass filter 510−550 nm, and the fluorescence signal of RITC was detected with a 560 nm long pass filter. Images were taken with a HCX PL APO lambda blue 63.0 × 1.40 oil-immersion objective and a pinhole aperture of 1 Airy unit.

■ ASSOCIATED CONTENT

Ⓢ Supporting Information

The calibration of capsule-based pH sensors (Figures S1 and S2); the detailed description of the tracking measurements and data analysis (Figures S3−S6); the mean velocity profile of capsule-based pH sensors during acidification (Figure S7); additional TEM images (Figures S8−S11). The Supporting Information is available free of charge on the ACS Publications website at DOI: 10.1021/acsami.5b04375.

■ AUTHOR INFORMATION

Corresponding Authors

*E-mail: cecilia.bucci@unisalento.it.

*E-mail: loretta.delmercato@nanotec.cnr.it.

Present Addresses

○P.R.-G. is currently at Department of Physical and Inorganic Chemistry, Rovira i Virgili University and the Chemistry Technology Center of Catalonia (CTQC), 43007 Tarragona, Spain.

△A.K. is currently at Plant Development, Department of Biology I, Biocenter LMU Munich, Grosshaderner Strasse 2−4, 82152 Planegg-Martinsried, Germany.

○M.M.F. and L.L.d.M. are currently at CNR NANOTEC−Istituto di Nanotecnologia, Polo di Nanotecnologia c/o Campus Ecotekne, Via Monteroni, 73100, Lecce, Italy.

Author Contributions

†These authors contributed equally. All authors have given approval to the final version of the manuscript.

Notes

The authors declare no competing financial interest.

■ ACKNOWLEDGMENTS

This work was partially supported by AIRC (Grant IG2013 N. 14709 to C.B.), by MIUR (PRIN2010-2011 to C.B.). R.R. and L.L.d.M. acknowledge the financial support from PON02_00563_3448479-F "RINOVATIS" and PONa3_00134 "ONEV". W.J.P. and A.K. acknowledge the LOEWE Research Cluster SynChemBio and the LOEWE Center for Synthetic Microbiology (SYNMIKRO), respectively. P.R.-G. acknowledges the Ministry of Economy and Competitiveness (RYC-2012-10059 & CTQ2013-45433-P) for

DOI: 10.1021/acsami.5b04375
ACS Appl. Mater. Interfaces 2015, 7, 15052−15060

financial support. Prof. Dr. Uwe-G. Maier is acknowledged for allocation of the EM facility and high-pressure freezer and Marion Debus for technical assistance.

REFERENCES

(1) Casey, J.; Grinstein, S.; Orlowski, J. Sensors and Regulators of Intracellular pH. *Nat. Rev. Mol. Cell Biol.* **2010**, *11*, 50−61.
(2) Weisz, O. A. Organelle Acidification and Disease. *Traffic* **2003**, *4*, 57−64.
(3) Mukherjee, S.; Ghosh, R. N.; Maxfield, F. R. Endocytosis. *Physiol. Rev.* **1997**, *77*, 759−803.
(4) Sun-Wada, G. H.; Wada, Y.; Futai, M. Diverse and Essential Roles of Mammalian Vacuolar-Type Proton Pump ATPase: Toward the Physiological Understanding of Inside Acidic Compartments. *Biochim. Biophys. Acta* **2004**, *1658*, 106−114.
(5) Marshansky, V.; Futai, M. The V-type H+-ATPase in Vesicular Trafficking: Targeting, Regulation and Function. *Curr. Opin. Cell Biol.* **2008**, *20*, 415−426.
(6) Whitten, S. T.; García-Moreno, E. B.; Hilser, V. J. Local Conformational Fluctuations Can Modulate the Coupling Between Proton Binding and Global Structural Transitions in Proteins. *Proc. Natl. Acad. Sci. U.S.A.* **2005**, *102*, 4282−4287.
(7) Kornak, U.; Reynders, E.; Dimopoulou, A.; van Reeuwijk, J.; Fischer, B.; Rajab, A.; Budde, B.; Nürnberg, P.; Foulquier, F.; Group, A. D.-t. S.; Lefeber, D.; Urban, Z.; Gruenewald, S.; Annaert, W.; Brunner, H. G.; van Bokhoven, H.; Wevers, R.; Morava, E.; Matthijs, G.; Van Maldergem, L.; Mundlos, S. Impaired Glycosylation and Cutis Laxa Caused by Mutations in the Vesicular H+-ATPase Subunit ATP6V0A2. *Nat. Genet.* **2008**, *40*, 32−34.
(8) Forgac, M. Vacuolar ATPases: Rotary Proton Pumps in Physiology and Pathophysiology. *Nat. Rev. Mol. Cell Biol.* **2007**, *8*, 917−929.
(9) Hinton, A.; Bond, S.; Forgac, M. V-ATPase Functions in Normal and Disease Processes. *Pflugers Arch.* **2009**, *457*, 589−598.
(10) del Mercato, L. L.; Ferraro, M. M.; Baldassarre, F.; Mancarella, S.; Greco, V.; Rinaldi, R.; Leporatti, S. Biological Applications of LbL Multilayer Capsules: from Drug Delivery to Sensing. *Adv. Colloid Interface Sci.* **2014**, *207*, 139−154.
(11) Kazakova, L.; Shabarchina, L.; Anastasova, S.; Pavlov, A.; Vadgama, P.; Skirtach, A.; Sukhorukov, G. Chemosensors and Biosensors Based on Polyelectrolyte Microcapsules Containing Fluorescent Dyes and Enzymes. *Anal. Bioanal. Chem.* **2013**, *405*, 1559−1568.
(12) Kreft, O.; Javier, A. M.; Sukhorukov, G. B.; Parak, W. J. Polymer Microcapsules as Mobile Local pH-Sensors. *J. Mater. Chem.* **2007**, *17*, 4471−4476.
(13) Munoz Javier, A.; Kreft, O.; Piera Alberola, A.; Kirchner, C.; Zebli, B.; Susha, A. S.; Horn, E.; Kempter, S.; Skirtach, A.; Rogach, A. L.; Radler, J.; Sukhorukov, G. B.; Benoit, M.; Parak, W. J. Combined Atomic Force Microscopy and Optical Microscopy Measurements as a Method to Investigate Particle Uptake by Cells. *Small* **2006**, *2*, 394−400.
(14) Ai, H.; Pink, J. J.; Shuai, X. T.; Boothman, D. A.; Gao, J. M. Interactions Between Self-Assembled Polyelectrolyte Shells and Tumor Cells. *J. Biomed. Mater. Res., Part A* **2005**, *73A* (3), 303−312.
(15) Reibetanz, U.; Halozan, D.; Brumen, M.; Donath, E. Flow Cytometry of HEK 293T Cells Interacting with Polyelectrolyte Multilayer Capsules Containing Fluorescein-Labeled Poly(acrylic acid) as a pH Sensor. *Biomacromolecules* **2007**, *8*, 1927−1933.
(16) Cortez, C.; Tomaskovic-Crook, E.; Johnston, A. P. R.; Radt, B.; Cody, S. H.; Scott, A. M.; Nice, E. C.; Heath, J. K.; Caruso, F. Targeting and Uptake of Multilayered Particles to Colorectal Cancer Cells. *Adv. Mater.* **2006**, *18*, 1998−2003.
(17) Zelikin, A. N.; Breheney, K.; Robert, R.; Tjipto, E.; Wark, K. Cytotoxicity and Internalization of Polymer Hydrogel Capsules by Mammalian Cells. *Biomacromolecules* **2010**, *11*, 2123−2129.
(18) Yan, Y.; Johnston, A. P. R.; Dodds, S. J.; Kamphuis, M. M. J.; Ferguson, C.; Parton, R. G.; Nice, E. C.; Heath, J. K.; Caruso, F. Uptake and Intracellular Fate of Disulfide-Bonded Polymer Hydrogel Capsules for Doxorubicin Delivery to Colorectal Cancer Cells. *ACS Nano* **2010**, *4*, 2928−2936.
(19) Muñoz Javier, A.; Kreft, O.; Semmling, M.; Kempter, S.; Skirtach, A. G.; Bruns, O. T.; del Pino, P.; Bedard, M. F.; Rädler, J.; Käs, J.; Plank, C.; Sukhorukov, G. B.; Parak, W. J. Uptake of Colloidal Polyelectrolyte-Coated Particles and Polyelectrolyte Multilayer Capsules by Living Cells. *Adv. Mater.* **2008**, *20*, 4281−4287.
(20) Kastl, L.; Sasse, D.; Wulf, V.; Hartmann, R.; Mircheski, J.; Ranke, C.; Carregal-Romero, S.; Martinez-Lopez, J. A.; Fernandez-Chacon, R.; Parak, W. J.; Elsasser, H. P.; Rivera-Gil, P. Multiple Internalization Pathways of Polyelectrolyte Multilayer Capsules into Mammalian Cells. *ACS Nano* **2013**, *7*, 6605−6618.
(21) Reibetanz, U.; Chen, M. H.; Mutukumaraswamy, S.; Liaw, Z. Y.; Oh, B. H.; Venkatraman, S.; Donath, E.; Neu, B. Colloidal DNA Carriers for Direct Localization in Cell Compartments by pH Sensoring. *Biomacromolecules* **2010**, *11* (7), 1779−1784.
(22) Song, X.; Li, H.; Tong, W.; Gao, C. Fabrication of Triple-Labeled Polyelectrolyte Microcapsules for Localized Ratiometric pH Sensing. *J. Colloid Interface Sci.* **2014**, *416*, 252−257.
(23) Zhang, P.; Song, X.; Tong, W.; Gao, C. Nanoparticle/Polymer Assembled Microcapsules with pH Sensing Property. *Macromol. Biosci.* **2014**, *14*, 1495−1504.
(24) Hartmann, R.; Weidenbach, M.; Neubauer, M.; Fery, A.; Parak, W. J. Stiffness-Dependent in Vitro Uptake and Lysosomal Acidification of Colloidal Particles. *Angew. Chem., Int. Ed.* **2015**, *54*, 1365−1368.
(25) Liang, K.; Gunawan, S. T.; Richardson, J. J.; Such, G. K.; Cui, J. W.; Caruso, F. Endocytic Capsule Sensors for Probing Cellular Internalization. *Adv. Healthcare Mater.* **2014**, *3* (10), 1551−1554.
(26) Rivera-Gil, P.; Nazarenus, M.; Ashraf, S.; Parak, W. J. pH-Sensitive Capsules as Intracellular Optical Reporters for Monitoring Lysosomal pH Changes Upon Stimulation. *Small* **2012**, *8*, 943−948.
(27) Ohira, M.; Smardon, A. M.; Charsky, C. M.; Liu, J.; Tarsio, M.; Kane, P. M. The E and G Subunits of the Yeast V-ATPaseInteract Tightly and Are Both Present at More than One Copy per V1 Complex. *J. Biol. Chem.* **2006**, *281*, 22752−22760.
(28) Tomashek, J. J.; Graham, L. A.; Hutchins, M. U.; Stevens, T. H.; Klionsky, D. J. V1-situated Stalk Subunits of the Yeast Vacuolar Proton-translocating ATPase. *J. Biol. Chem.* **1997**, *272*, 26787−26793.
(29) De Luca, M.; Bucci, C. A New V-ATPase Regulatory Mechanism Mediated by the Rab Interacting Lysosomal Protein (RILP). *Commun. Integr. Biol.* **2014**, *7*, 1−4.
(30) De Luca, M.; Cogli, L.; Progida, C.; Nisi, V.; Pascolutti, R.; Sigismund, S.; Di Fiore, P. P.; Bucci, C. The Rab-Interacting Lysosomal Protein (RILP) Regulates Vacuolar ATPase Acting on the V1G1 Subunit. *J. Cell Sci.* **2014**, *127*, 2697−2708.
(31) del Mercato, L. L.; Abbasi, A. Z.; Parak, W. J. Synthesis and Characterization of Ratiometric Ion-Sensitive Polyelectrolyte Capsules. *Small* **2011**, *7*, 351−363.
(32) del Mercato, L. L.; Abbasi, A. Z.; Ochs, M.; Parak, W. J. Multiplexed Sensing of Ions with Barcoded Polyelectrolyte Capsules. *ACS Nano* **2011**, *5*, 9668−9674.
(33) Decher, G. Fuzzy Nanoassemblies: Toward Layered Polymeric Multicomposites. *Science* **1997**, *277*, 1232−1237.
(34) Sukhorukov, G. B.; Donath, E.; Lichtenfeld, H.; Knippel, E.; Knippel, M.; Budde, A.; Mohwald, H. Layer-by-Layer Self Assembly of Polyelectrolytes on Colloidal Particles. *Colloids Surf., A* **1998**, *137*, 253−266.
(35) Carregal-Romero, S.; Rinklin, P.; Schulze, S.; Schafer, M.; Ott, A.; Huhn, D.; Yu, X.; Wolfrum, B.; Weitzel, K. M.; Parak, W. J. Ion Transport Through Polyelectrolyte Multilayers. *Macromol. Rapid Commun.* **2013**, *34*, 1820−1826.
(36) Antipov, A. A.; Sukhorukov, G. B.; Mohwald, H. Influence of the Ionic Strength on the Polyelectrolyte Multilayers' Permeability. *Langmuir* **2003**, *19*, 2444−2448.
(37) Sukhorukov, G. B.; Brumen, M.; Donath, E.; Mohwald, H. Hollow Polyelectrolyte Shells: Exclusion of Polymers and Donnan Equilibrium. *J. Phys. Chem. B* **1999**, *103*, 6434−6440.

DOI: 10.1021/acsami.5b04375
ACS Appl. Mater. Interfaces 2015, 7, 15052−15060

(38) Murphy, R. F.; Powers, S.; Cantor, C. R. Endosome pH Measured in Single Cells by Dual Fluorescence Flow Cytometry: Rapid Acidification of Insulin to pH 6. *J. Cell Biol.* **1984**, *98*, 1757−1762.
(39) Haas, A. The Phagosome: Compartment with a License to kill. *Traffic* **2007**, *8*, 311−330.
(40) Sukhorukov, G. B.; Rogach, A. L.; Zebli, B.; Liedl, T.; Skirtach, A. G.; Kohler, K.; Antipov, A. A.; Gaponik, N.; Susha, A. S.; Winterhalter, M.; Parak, W. J. Nanoengineered Polymer Capsules: Tools for Detection, Controlled Delivery, and Site-Specific Manipulation. *Small* **2005**, *1*, 194−200.
(41) Palankar, R.; Pinchasik, B. E.; Schmidt, S.; De Geest, B. G.; Fery, A.; Mohwald, H.; Skirtach, A. G.; Delcea, M. Mechanical Strength and Intracellular Uptake of $CaCO_3$-Templated LbL Capsules Composed of Biodegradable Polyelectrolytes: the Influence of the Number of Layers. *J. Mater. Chem. B* **2013**, *1*, 1175−1181.
(42) Rivera-Gil, P.; De Koker, S.; De Geest, B. G.; Parak, W. J. Intracellular Processing of Proteins Mediated by Biodegradable Polyelectrolyte Capsules. *Nano Lett.* **2009**, *9*, 4398−4402.
(43) Pols, M. S.; van Meel, E.; Oorschot, V.; ten Brink, C.; Fukuda, M.; Swetha, M. G.; Mayor, S.; Klumperman, J. hVps41 and VAMP7 Function in Direct TGN to Late Endosome Transport of Lysosomal Membrane Proteins. *Nat. Commun.* **2013**, *4*, 1361.
(44) Luzio, J. P.; Pryor, P. R.; Bright, N. A. Lysosomes: Fusion and Function. *Nat. Rev. Mol. Cell Biol.* **2007**, *8*, 622−632.
(45) del Mercato, L. L.; Gonzalez, E.; Abbasi, A. Z.; Parak, W. J.; Puntes, V. Synthesis and Evaluation of Gold Nanoparticle-Modified Polyelectrolyte Capsules under Microwave Irradiation for Remotely Controlled Release for Cargo. *J. Mater. Chem.* **2011**, *21*, 11468−11471.

DOI: 10.1021/acsami.5b04375
ACS Appl. Mater. Interfaces 2015, 7, 15052−15060